Iron redox effect on the structure and viscosity of silicate glasses and melts

Sohei Sukenaga, Maria Rita Cicconi, Hiroki Yamada, Toru Wakihara, Koji Ohara, Hiroyuki Shibata, Daniel Neuville

Iron redox effect on the structure and viscosity of silicate glasses and melts

Sohei Sukenaga,[1,2]* Maria Rita Cicconi,[2,3] Hiroki Yamada,[4] Toru Wakihara,[5] Koji Ohara,[6] Hiroyuki Shibata[1], and Daniel R. Neuville[2]*

[1] Institute of Multidisciplinary Research for Advanced Materials (IMRAM), Tohoku University, 2-1-1 Katahira, Aoba-ku, 9808577 Sendai, Japan

[2] Geomatériaux, IPGP, CNRS, USPC, 1 rue Jussieu, 75005 Paris, France

[3] Institute of Glass and Ceramics, Department of Materials Science and Engineering, Friedrich-Alexander-Universität Erlangen-Nürnberg, Martensstr. 5, D-91058 Erlangen, Germany.

[4] Research Utilization Division, Japan Synchrotron Radiation Research Institute (JASRI/Spring-8), 111 Kouto, Sayo-cho, 6795198 Hyogo, Japan

[5] Institute of Engineering Innovation, School of Engineering, The University of Tokyo, Yayoi 2-11-16, Bunkyo-ku, 1138656 Tokyo, Japan

[6] Faculty of Materials for Energy, Shimane University, 1060 Nishikawatsu-cho, 6908504 Matsue, Japan

***Corresponding authors:**

Sohei Sukenaga: sohei.sukenaga.d3@tahoku.ac.jp

Daniel R. Neuville: neuville@ipgp.fr

Abstract

The viscosity of silicate melts is one of the most important physical properties for understanding high-temperature phenomena in magmatic systems as well as materials processing. The effects of composition and temperature on viscosity have long been elucidated. Although iron ions are a main component of the magmatic system, their influence on viscosity remains unclear because the behavior of iron is complicated; iron ions have two redox states, that is, Fe^{3+} and Fe^{2+}. Here, we elucidate the viscosity of an iron-sodium-silicate system with a variety of iron redox states at temperatures close to its glass transition (T_g). The redox states and structures of the samples were characterized using X-ray absorption near-edge structure (XANES) spectroscopy, Raman spectroscopy, synchrotron X-ray total scattering, and density (molar volume) measurements. The viscosity increased (by more than two orders of magnitude) with an increase in the ratio of Fe^{3+} to total Fe (Fe^{3+}/Fe^{tot}) whereas the temperature dependence of the viscosity was larger for glasses with a higher Fe^{3+}/Fe^{tot} ratio. The tendencies in viscosity and structural variation against the Fe^{3+}/Fe^{tot} ratio support the consensus on the structural roles of Fe^{3+} and Fe^{2+} from previous studies: Fe^{3+} ions have a stronger tendency to behave as a network former than Fe^{2+} ions. (202 words)

Keywords: viscosity; fragility; molar volume; silicate melts; iron redox state; X-ray absorption spectroscopy; synchrotron X-ray total scattering; supercooled liquid

1 Introduction

The viscosity of silicate liquids is important for understanding the role of silicate liquids in Earth's mass transfer for the dynamism of volcanic eruptions at elevated temperatures.[1] Viscosity is a key property for controlling the fluidity and crystallization behavior of silicate liquids, which is also important in high-temperature industries such as metallurgical extraction (as slags)[2] and the fabrication of glass-ceramics.[3] Owing to their importance, viscosities have been extensively investigated in simple two- or three-component systems[4–9] and in more complex systems.[10–13] Some models[14] have approximately reproduced their empirical variations. More recently, Le Losq and Neuville[15] have shown that using the knowledge of the glass structure from NMR or Raman spectroscopy, it is possible to establish a viscosity model quite accurately for a wide temperature range but working only for simple binary or ternary systems. Giordano and Russell developed a viscosity model based on the empirical linkage between the Raman spectra and viscosity data.[16] In all these studies, one of the most important elements for earth[17] and materials science[18] is missing: iron. Because it is difficult to investigate its structural role in silicate systems. Iron can play different roles depending on the chemical composition, temperature, and oxygen fugacity.[19] It can act as a charge compensator or network modifier, such as Ca^{2+} when iron is divalent (Fe^{2+}) or as a network former, such as Al^{3+}, when iron is present as a trivalent cation (Fe^{3+}). This chemical change in the redox state

of iron can produce significant changes in viscosity at high temperatures, that is, above the liquidus, as shown by previous studies.[20, 21] The need for Fe^{3+} as a charge compensator has recently been demonstrated by X-ray absorption near edge structure (XANES) spectroscopy at the Ca K-edge[22] which confirms its role as a network former. In situ high-temperature Mössbauer spectra[23] have shown that the relaxation times around Fe^{2+} and Fe^{3+} are different, and a wider variation in the viscosity by changing the redox state of iron can be expected in the lower-temperature region close to the glass transition. A few researchers have evaluated its effect on the viscosity of supercooled liquids using multicomponent samples whose compositions are close to those of natural samples.[24–27] However, the mechanism of the viscosity change against the redox state of iron remains ambiguous because the structural characterization of a multicomponent system is difficult. Although some studies have reported the viscosity of a simpler iron-silicate system with two or three levels of redox states,[28–30] the effect of iron redox on silicate viscosity has not been studied systematically for a wide variety of temperatures and iron redox states along with their structural changes.

In the present study, the viscosity change with variation in the iron redox state was measured at temperatures close to the glass transition, that is, supercooled liquids, for a chosen sodium-iron-silicate system. One of the authors reported the viscosity of this system in a higher temperature range above the liquidus.[31] The viscous behavior of an iron sodium silicate liquid with a variety of iron redox states has been reported over a wide temperature range. X-ray absorption spectroscopy, Raman spectroscopy, synchrotron X-ray diffraction,

and density (molar volume) measurements were performed to evaluate the redox states and structures of the samples. The structural roles of Fe^{3+} and Fe^{2+} are discussed based on their measured properties and structural information.

2 Experimental method

2.1 Glass Synthesis

Reagent powders of SiO_2, Na_2CO_3 and Fe_2O_3 were precisely weighed to obtain the target composition of 30 mol%Na_2O–60mol%SiO_2–10mol%Fe_2O_3 (NSF). The powder mixtures were placed in a platinum crucible and melted for 20 min in air. The melts were then quenched using a Cu plate. The quenched samples were crushed into powders, and a portion of the powder (approximately 6 g) was placed in a Pt crucible. Subsequently, to change the sample redox state, the quenched samples were remelted for 270 min at 1773 K in three different atmospheres with a variety of oxygen partial pressures: O_2, Air, Argon and Ar-1%H_2. Hereinafter, the samples were referred as “NSF_O2,” “NSF_Air,” “NSF_Argon,” “NSF_Ar/H2” in this paper. The melts were cast into a BN-coated graphite mold, and the obtained bubble-free glassy samples were annealed for 12 h in air at temperatures of 20-40 K below their glass transition. The annealed samples were then shaped into cylinders (diameter: 4-5 mm, height: 8-10 mm). The cylindrical samples were used for the viscosity measurements at temperatures close to glass transition and density measurements at room temperature (R.T.: 303 ± 1 K). In addition, samples with the same thermal histories were used for structural characterization. The densities (d) of the glass samples were measured using Archimedes’ method at room temperature. Toluene was used as the immersion liquid and the

measurements were repeated three times for each sample. To compare the structural densities of the samples, their molar volumes (V_{m}) at R.T. were obtained using Eq.(1):

$$V_{\mathrm{m}} = \frac{M}{d}, \quad (1)$$

where M denotes the total molar mass of the sample. For V_{m} calculations, two iron species (ferric and ferrous) were considered separately according to the Fe redox ratios estimated by X-Ray Absorption Spectroscopy (see below). The obtained V_{m} values are listed in **Table 1**.

The elemental composition of the samples was determined by wet-chemical analysis, the Si and Fe oxide concentrations were determined using inductively coupled plasma atomic emission spectroscopy (ICP-AES) and SiO_2 gravimetric analysis, and the Na concentration was quantified using atomic absorption spectrometry (AAS). 33.3 mol%Na_2O–66.7 mol%SiO_2 (NS66.0) glass, which was prepared by a conventional melt-and-quench method, was used for Raman and synchrotron X-ray scattering experiments.

Table 1 Analyzed compositions (as mol%, recalculated from wet chemical analysis) and properties of the glasses. The nominal composition should be 54.6SiO_2–27.2Na_2O–18.2FeO (mol%) when iron oxide concentration is calculated as FeO.

	O_2	Air	Argon	ArH_2
SiO_2	54.8	55.5	54.8	56.7
Na_2O	27.1	26.4	26.9	26.6
FeO_{tot} [a]	18.1	18.1	18.3	16.7
Fe^{3+}/Fe^{tot} [b]	0.95(5)	0.85(5)	0.60(5)	0.38(5)
Si/Fe [c]	3.0	3.1	3.0	3.4
d (g/cm^3)	2.755(2)	2.768(3)	2.782(2)	2.817(1)
V_{m} (cm^3/mol) [d]	25.5	25.1	24.2	23.1

[a] total content of iron oxide as FeO, determined using ICP analysis.

[b] the ratio of Fe^{3+} to total Fe determined by Fe-K edge XAS spectroscopy (± 0.05)
[c] atomic ratio
[d] Molar volume of the glasses derived from density and chemical composition.

2.2 Viscosity measurements

Viscosity measurements of the supercooled liquids were conducted in air using the creep apparatus described by Neuville.[7] Using this apparatus, a load up to 500 kg was applied to each sample. For a 3 mm diameter sample, the maximum stress was 700×10^6 $N\cdot m^{-2}$, and for a 9 mm diameter sample the stress was 80×10^6 $N\cdot m^{-2}$. The temperature gradient is an important parameter for these measurements. Therefore, a silver cylinder attached to the upper piston is used to reduce the temperature gradient of the sample. The temperature was measured using two Pt-Pt/Rh10% thermocouples placed at the top and bottom of the sample. The temperature difference along the cylinder is less than 0.2 K. The sample used for the measurement was cylindrical with 4-5 mm diameter and 8-10 mm length and an approximate weight of 0.5 g. By comparing with the reported values of relaxed viscosity on SRM 710 glass from the National Bureau of Standards, we estimated the viscosity uncertainty and reproducibility to be less than 0.03 log units with this technique (see ref. 7). Within the range of stress applied in the creep experiment (6.6-8.9 log $N\cdot m^{-2}$), the viscosity of the samples was Newtonian.

2.3 Fe K-edge XANES

XANES spectroscopy data were collected at the LUCIA beamline (SOLEIL, F) using a Si_{311} crystal monochromator in fluorescence mode (SDD), with the sample surface placed at 5–7 °with respect to the incoming beam to avoid self-absorption. The energy range scanned was from 7000 to 7400 eV in step-scan mode, with the region 7108 to 7118.5 eV scanned with a step energy of 0.1 eV, and the absorption edge (7118.5–7140 eV) by using a step energy of 0.5 eV. The average of the three spectra was obtained, and the energy was calibrated using Fe foil (7112 eV). Three Fe crystalline compounds (aegirine, staurolite, and hematite) were also analyzed as finely crushed powders spattered on carbon tape. XANES data reduction has been described in detail by Cicconi et al.[32]

2.4 Raman spectroscopy

Measurements were performed using a T64000 Horiba Raman spectrometer equipped with a CCD detector. The 488.1 nm line of a Coherent 70-C5 Ar^+ laser operating at 200 mW was used for sample excitation. For the examined samples, this excitation and CCD system yielded a signal-to-noise ratio of 80/1. The integration time was 60s. With our triple spectrometer, it is possible to take spectra at very low frequency (less than 10 cm^{-1}). All reported spectra were unpolarized.

2.5 Synchrotron X-ray total scattering

Synchrotron X-ray total scattering was measured using the high-energy X-ray diffraction facility at Spring-8 (BL04B2, Japan). The crushed glass powders were packed in

Kapton capillary tubes (diameter: 3-3.5 mm) and the scattering patterns of the samples were collected by a horizontal 2-axis diffractometer under the vacuum condition at room temperature with the energy of incident X-ray of 61.4 keV (λ = 0.202 Å). Scattering vector (q) is described as q = 4πsinθ/λ. The highest q value for the present study is 26 $Å^{-1}$. To obtain the Faber-Ziman structure factor ($S(q)$), scattering patterns were handled according to a well-established procedure.[33] In an X-ray scattering experiment on glass containing n chemical components, the total structure factor $S(q)$ is represented by Eq. (2):[34]

$$S(q) = 1 + \frac{1}{|<w(q)>|^2}\sum_{\alpha=1}^{n}\sum_{\beta=1}^{n} c_\alpha c_\beta\, w_\alpha(q) w_\beta(q)[S_{\alpha\beta}(q) - 1], \quad (2)$$

where c_α is the atomic fraction of chemical component α; $w_\alpha(q)$ is a q independent atomic form factor with dispersion terms in X-ray scattering; $S_{\alpha\beta}(q)$ is a partial structure factor; $|<w(q)>|^2 = \sum_{\alpha=1}^{n}\sum_{\beta=1}^{n} c_\alpha c_\beta\, w_\alpha(q) w_\beta(q)$. To determine the interatomic distance between the iron and oxygen atoms, the total correlation function $T(r)$ was obtained from the Fourier transform Eqs. (3) and (4):

$$T(r) = 4\pi r \rho_0 g(r)\ , \quad (3)$$

$$g(r) = 1 + \frac{1}{2\pi^2 \rho_0 r}\int_{q_{min}}^{q_{max}} q[S(q) - 1]\sin(qr)dq, \quad (4)$$

where ρ_0 [m^{-3}] is a number of atoms in a unit volume and $g(r)$ is a weighted sum of partial functions.

3 Results

3.1 Chemical compositions, densities and redox state of the samples

The results of the compositional analyses are listed in Table 1. The atomic ratios of Si to Fe (Si/Fe) are listed in Table 1, and the values agree with the nominal ratio (3.0) for samples melted under O_2, air, and Ar atmospheres. However, the NSF_Ar/H2 sample had a slightly larger ratio (Si/Fe = 3.4), suggesting that a small portion of iron was lost during synthesis under the most reducing conditions (Ar-1%H_2 atmosphere). This explains the lower Fe content in NSF_Ar/H2 (Table 1).

The normalized Fe K-edge X-ray absorption near edge structure (XANES) spectra of the four glasses are shown in **Figure 1 a)**. As expected, the different synthesis conditions induced variations in the main edge position and shape because of the different Fe^{3+}/Fe^{tot} ratios. The Fe main edge shifts from 7123.5 eV (under O_2) to 7119.5 eV (under Ar/H_2), and the respective pre-edge peak barycenter (centroid) shifts as well toward lower energies by decreasing the Fe^{3+}/Fe^{tot} ratio (Figure 1b) because of the relative increase of the lower component, related to Fe^{2+} species. Deconvolution of the pre-edge peaks was performed according to the procedure reported by Cicconi et al.[32] and the Fe redox ratio was evaluated for all the spectra (see Table 1).

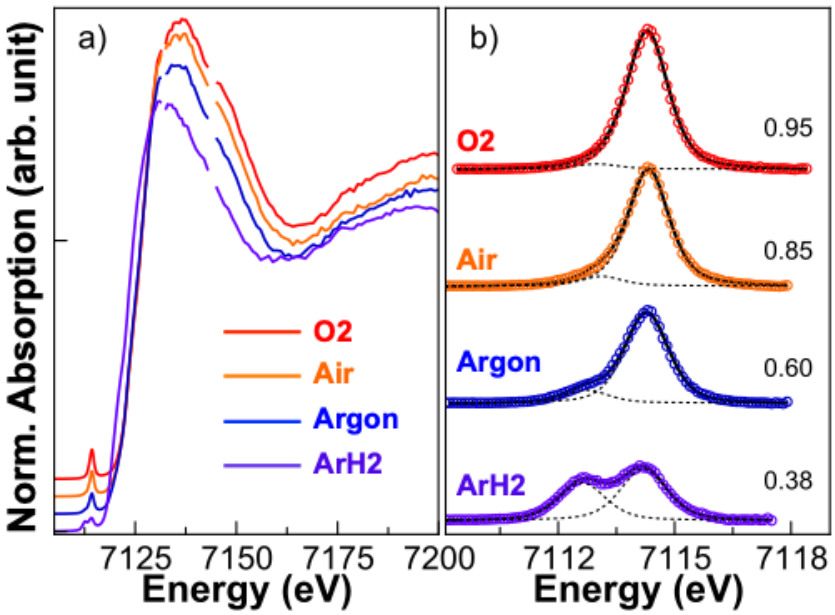

Figure 1 a) XANES at the Fe K-edge of the NSF glasses, obtained at room temperature. b) Fitting results of the pre-edge peak of the XANES spectra. Numbers on the figure displays the ratio of Fe^{3+} to total-iron (Fe^{3+}/Fe^{tot}).

The volume properties of the samples are listed in Table 1. The density values systematically decreased in the order of NSF_Ar/H2 > NSF_Argon > NSF_Air > NSF_O2, in agreement with the increase in Fe^{3+} species. Based on the proportions of Fe^{2+} and Fe^{3+} estimated by XANES analysis, the molar volume (V_m) of each glass was determined. The V_m values increased nearly linearly with increasing Fe^{3+}/Fe^{tot} ratio.

3.2 Viscosity

The viscosities (η) of the Na_2O–SiO_2–FeO–Fe_2O_3 supercooled liquids with variations in the iron redox state are listed in **Table 2 a)**. For the viscosity at temperatures above their liquids, we employed the reported viscosity of the same system under similar atmospheric conditions at 1773 K.[31] Because Osugi[31] reported that the viscosity became almost constant by melting for 120-165 min under each atmosphere, the plateau viscosity values at each atmosphere were used in the present study (see Table 2 b)).

These data are plotted against the reciprocal temperature ($1/T$) in Figure 2, where the logarithmic viscosities increase linearly with increasing $1/T$ in the lower temperature range (i.e., temperatures close to glass transition ($\log \eta = 12$)) for all samples. The slope of the linear relationship (i.e., the apparent activation energy for viscous flow) was comparable for

NSF_O2, NSF_Air, and NSF_Argon; however, the slope for NSF_ArH2 was smaller than those of the other samples. In addition, the viscosity of the samples strongly depended on the type of atmosphere used for the melting process; the viscosity was in the order of NSF_O2 > NSF_Air > NSF_Argon > NSF_ArH2 at a comparable temperature. A similar tendency was observed at temperatures close to the glass transition temperature for sodium-iron-silicate[28,29] and sodium iron aluminosilicate[29] as well and more complex silicate systems.[10, 25–27]

For a wide temperature range, from temperatures close to the glass transition to temperatures above their liquidus, the viscosity of the silicate melts varied non-linearly against 1/*T*. Figure 2 shows the viscosity data of the given Na_2O–SiO_2–FeO–Fe_2O_3 system, compared with that for the 33.3 mol%Na_2O–66.6 mol%SiO_2 (NS66.0) reported by Neuville.[7] As shown in Figure 2, the viscosity of the Na_2O–SiO_2–FeO–Fe_2O_3 system was lower than that of NS66.0, indicating that the addition of iron oxide decreased the viscosity of the sodium silicate melts. It should be noted that the viscosity of the Na_2O–SiO_2–FeO–Fe_2O_3 system changed slightly depending on the melting atmosphere at a higher temperature, that is 1773 K, whereas the viscosity variation greatly increased as the temperature decreased.

To determine the structural variation of sodium iron silicate glasses with the change in the iron redox state, the glass samples were characterized using Raman spectroscopy and synchrotron X-ray total scattering.

Table 2

a) Viscosity measurements at low temperature, temperature in Kelvin, and viscosity in log Pa·s.

O_2		Air		Argon		ArH_2	
T(K)	log η	*T*(K)	log η	*T*(K)	log η	*T*(K)	log η
771.1	8.95	751.1	8.93	737.9	8.78	702.3	9.16
760.6	9.50	746.7	9.21	732.7	9.07	700.7	9.23
753.0	9.89	741.2	9.49	728.8	9.32	694.9	9.54
745.8	10.31	736.1	9.77	723.9	9.59	685.6	10.12
736.2	10.92	730.5	10.13	719.3	9.88	680.1	10.42
731.1	11.24	727.8	10.29	714.3	10.20	672.9	10.84
726.8	11.54	721.3	10.70	711.8	10.34	670.4	11.00
720.8	11.94	717.9	10.93	709.4	10.52	666.0	11.24
715.4	12.31	713.2	11.23	706.3	10.71	659.1	11.67
710.5	12.64	710.7	11.41	704.4	10.86	653.3	12.05
		710.2	11.42	703.3	10.92	651.3	12.18
		707.6	11.65	699.6	11.20	648.0	12.39
		702.8	11.96	694.7	11.55		
		699.3	12.21	689.6	11.92		
		697.0	12.41	686.9	12.11		
				684.8	12.27		

b) Viscosities at high temperature (1773 K) reported by Osugi et al.[31]

O_2		Air		Argon		ArH_2	
T(K)	log η	*T*(K)	log η	*T*(K)	log η	*T*(K)	log η

1773	–0.161*	1773	–0.180	1773	–0.270	1773	–0.314

*Viscosity in pure O_2 atmosphere was estimated by extrapolation.

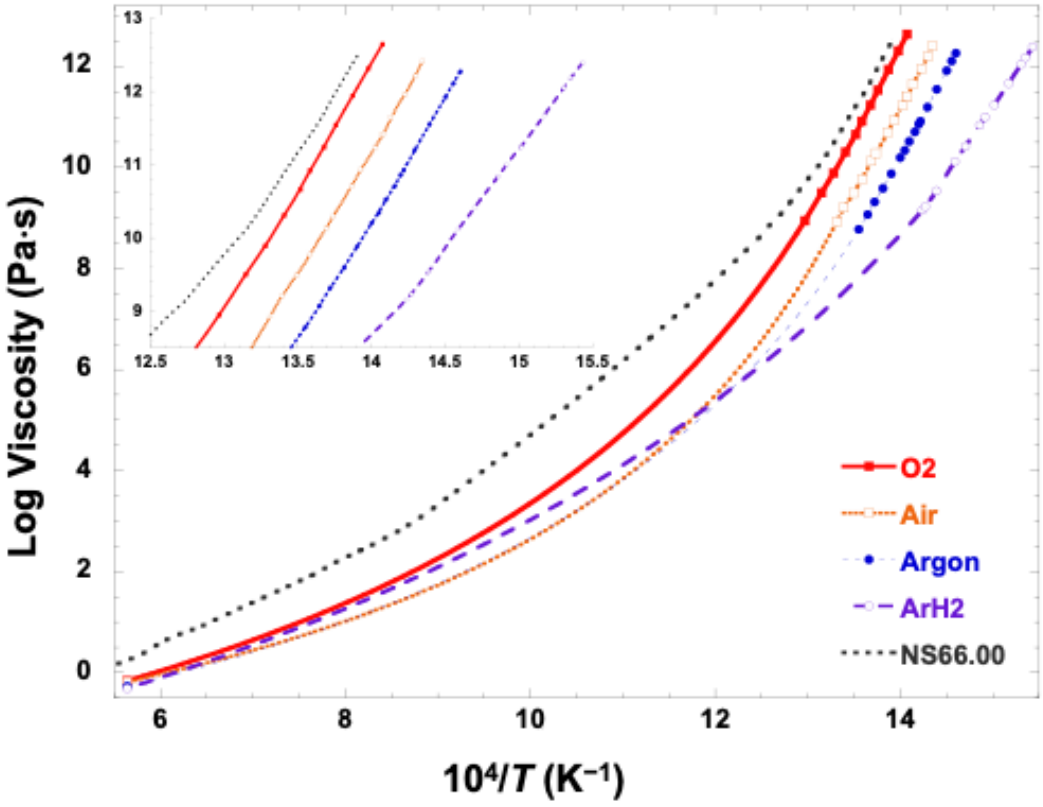

Figure 2 Viscosities of the sodium-iron-silicate melts as a function of reciprocal temperature. Literature data[7] of NS66.0 is plotted for comparison. Inset: logarithmic viscosity vs reciprocal temperature near glass transition.

3.4 Raman spectra

The Raman spectra of the samples are shown in Figure 3. In general, the Raman spectra of silicate glasses can be divided into four regions:[35] i) the boson region (25-250

cm^{-1}), ii) low-frequency region (250-700 cm^{-1}), iii) medium-frequency region (700-850 cm^{-1}), and iv) high-frequency region (850-1200 cm^{-1}). We consider in more detail some of these frequency regions to describe the structural modifications occurring in the glasses by varying the Fe redox ratio.

3.4.1 The boson region

The Raman spectra of glass materials show an asymmetric broad band in the lower-frequency region (25-250 cm^{-1}). This band, referred as "boson peak," is related to the intermediate structure of the glasses. To evaluate the position of peak maximum (ω_{BP}), the spectra was fitted using a "long-normal curve," shown in eq. (5):[36]

$$I(\omega) = I_{BP} \cdot exp\left(-\frac{(ln\omega - ln\omega_{BP})^2}{\sigma^2}\right), \quad (5)$$

where I_{BP} is the peak intensity, ω_{BP} the peak position, and σ indicates the full width at half maximum (FWHM) of the boson peak. The derived ω_{BP} by the fitting increased in the following order: NSF_O_2 (93 cm^{-1}) > NSF_ArH2 (90 cm^{-1}) > NSF_Air (75 cm^{-1}) > NSF_Argon (65 cm^{-1}). The σ values were approximately 2.2 cm^{-1} for all samples.

3.4.2 Low frequency region

Broad asymmetric bands close to 400-700 cm^{-1} has been assigned to bending vibration of bridging oxygens (BOs) associated with three-, four-, five-, six-, or higher-membered rings of tetrahedral units in the silicate network structure.[35] The Raman spectrum of an Fe-free NS66.0 glass is reported as a reference in Figure 3A and shows the

typical vibrational bands for this composition.[37] The main band in the low frequency region is a sharp asymmetric peak at approximately 570 cm^{-1} associated to T–O–T vibrations (where T represents framework cations, *i.e.* Si). The introduction of iron into the Na-silicate network induced variations in the position and shape of the main bands in the low-frequency region, and the prevalent presence of ferrous or ferric iron produced dissimilar changes in the Raman spectra.

3.4.4 High-frequency region

Raman vibrations in the high-frequency region (850-1200 cm^{-1}) are derived from the T–O stretching vibration in different Q^n tetrahedral units (Q represents a Si-centered tetrahedron and n the number of bridging oxygen atoms; n= 0–4). The high frequency envelope of the iron-free NS66.0 glass has two visible peaks: the strong band, peaking at 1100 cm^{-1}, and the smaller contribution at ~ 945 cm^{-1}, that are associated to different Q^n tetrahedral units where Si occurs mainly in Q^3 and Q^2 units, with only a small contribution from Q^4 units, in agreement with previous studies.[35,38]

The presence of iron in the Na-silicate glass induces strong modifications in the high frequency envelop, with a broader peak at 1100 cm^{-1} and the appearance of another contribution approximately at 900 cm^{-1}. The latter has been assigned to the antisymmetric mode of coupled $Fe^{3+}O_4$–SiO_4 tetrahedra,[39–45] reflecting the occurrence of four-fold coordinated Fe^{3+} species. The intensity of the peak at 900 cm^{-1} increased with the oxidation of Fe ions in the glasses.

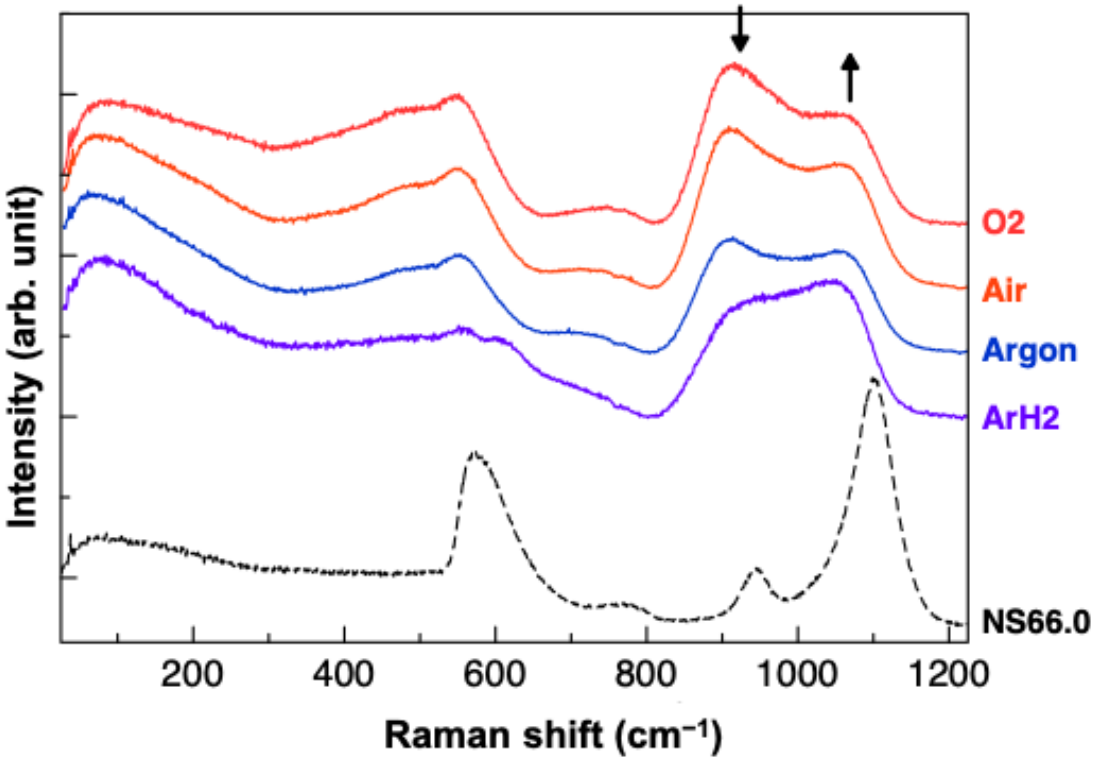

Figure 3 Raman spectra of the Na_2O–SiO_2–Fe_xO (NSF) glasses, which were prepared in a variety of atmospheres, compared with that of NS66.0 glass.

3.5 Synchrotron X-ray total scattering

Figure 4 displays the total correlation function ($T(r)$) for the NSF glasses compared with that of NS66.0 glass. In the NS66.0 glass, peaks at 1.6 Å, 2.3 Å and 2.6 Å are assigned to Si–O, Na–O and O–O correlation, respectively.[46] When iron oxide was added to the Fe-free sodium silicate glass, no significant change is observed in Si–O correlation while Fe–O correlation peak is found at 1.8-2.1 Å.[46] Interatomic distance of Fe–O ($L_{\mathrm{Fe-O}}$) varies depending on the melting atmosphere. Gaussian fit to the Fe–O correlation shows that

$L_{\mathrm{Fe-O}}$ is systematically become longer in the order of NSF_Ar/H2 (2.00 Å) > NSF_Argon (1.96 Å) > NSF_Air (1.93 Å) > NSF_O_2 (1.91 Å). In addition, the peak position and intensity of the Na–O correlation in the NSF glasses broadened in the order NSF_Ar/H_2 > NSF_Argon > NSF_Air > NSF_O_2.

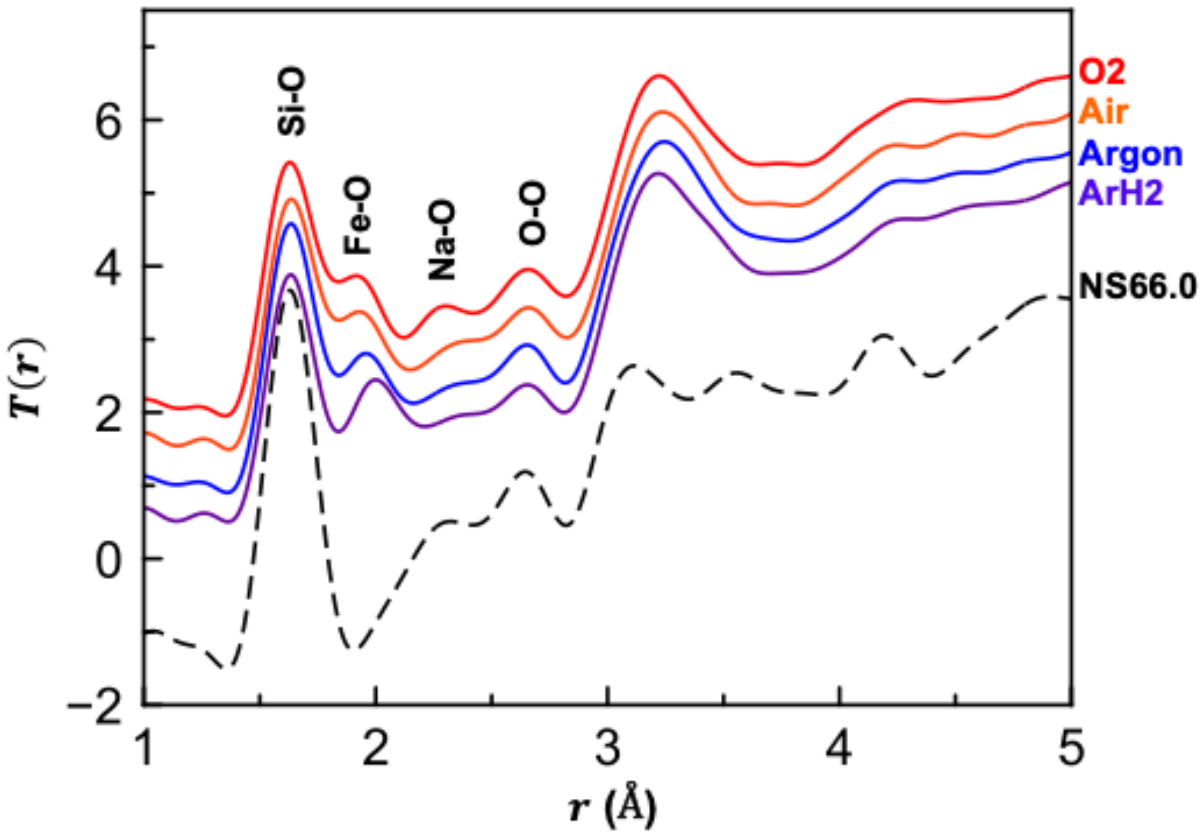

Figure 4 Total correlation function ($T(r)$) of the NSF glasses, compared with that of NS66.0 glass at room temperature.

4 Discussion

4.1 Interatomic distance between iron and oxygen

The local structure of iron ions in silicate glasses and melts is complicated because iron has two redox states, and the coordination numbers of both Fe^{3+} and Fe^{2+} can change in

the range of 4-6 depending on the temperature and chemical composition. Nuclear magnetic resonance spectroscopy enables the quantification of the coordination number for some framework cations (e.g., Si^{4+}, Al^{3+}) in silicate glasses,[47,48] however, it is still difficult to quantify each iron site with different redox states and coordination numbers in silicate glasses. Recently, the average coordination number of iron ions was associated with the Fe–O interatomic distance ($L_{\mathrm{Fe-O}}$) using XANES, neutron diffraction, and synchrotron X-ray total scattering for iron-containing glasses and crystals.[46,49–51] Figure 5 shows $L_{\mathrm{Fe-O}}$ of the NSF glasses as a function of the Fe^{3+}/total Fe ratio. $L_{\mathrm{Fe-O}}$ linearly decreases with oxidation of iron ions. Although it is difficult to make iron silicate glasses with a single type of iron cation (i.e., Fe^{3+} or Fe^{2+}), an extrapolation of the linear relation in Figure 5 allows us to estimate $L_{\mathrm{Fe-O}}$ at two extreme conditions: $L_{\mathrm{Fe-O}}$ at Fe^{3+}/Fe^{tot} = 0 and 1. Obtained $L_{\mathrm{Fe-O}}$ at Fe^{3+}/Fe^{tot} = 1 is 1.90 Å, indicating average coordination number of Fe^{3+} in the sodium silicate glass is in between 4 and 5 because calculated $L_{\mathrm{Fe-O}}$ for Fe^{3+} in 4-fold and 5-fold coordination are 1.85 Å and 1.94 Å, respectively.[51] This result is consistent with those of previous studies on iron–sodium–silicate glasses.[52] $L_{\mathrm{Fe-O}}$ for the NSF glass at Fe^{3+}/Fe^{tot} = 0 will be close to 2.06 Å by extrapolation of the linear relationship in Figure 5. Jackson et al.[50] suggested a relationship between $L_{\mathrm{Fe-O}}$ and the number of nearest neighbors (NN) for Fe^{2+}; $NN = -18.2 + 11.28 \cdot L_{\mathrm{Fe-O}}$. This equation gives an *NN* of 5.0 for Fe^{2+} in sodium silicate glass. The obtained $L_{\mathrm{Fe-O}}$ indicates that Fe^{3+} ions exist mainly in 4-fold or 5-fold coordination, whereas the average coordination number of Fe^{2+} is close to 5 for the chosen sodium silicate glasses.

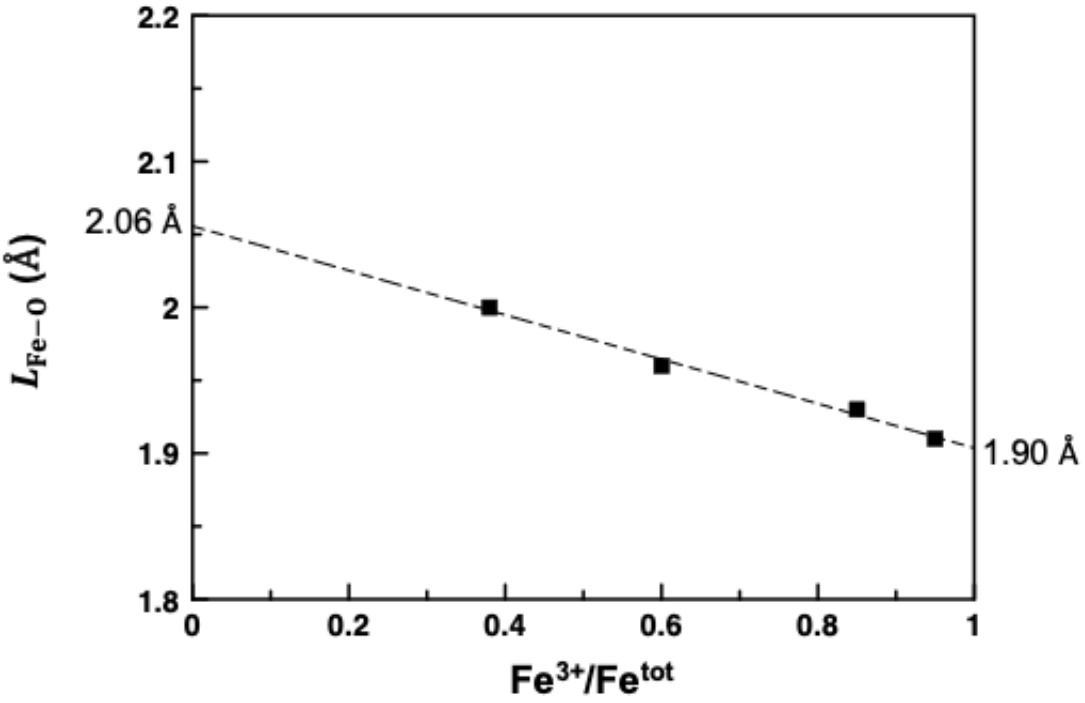

Figure 5 Influence of iron redox state (Fe^{3+}/Fe^{tot}) on the interatomic distance between iron and oxygen (L_{Fe-O}) in the NSF glasses at room temperature. The L_{Fe-O} was determined by a Gaussian fit to the $T(r)$. The numbers in the figure shows the estimated L_{Fe-O} at the two end points when Fe^{3+}/Fe^{tot} = 0 and 1.

4.2 Effect of iron redox state on V_m

Figure 6 shows the evolution of the molar volume (V_m) and glass transition temperature (T_g) with variations in the Fe^{3+}/Fe^{tot} ratio. *The* V_m of the NSF glasses increased with increasing Fe^{3+}/Fe^{tot} ratio, indicating that the NSF glasses became less dense owing to the oxidation of iron ions. This tendency goes against reported values for $Na_2Si_3O_7$–Fe_xO glasses with the smaller concentration of Fe oxides (ca. 5 mol% of iron oxide as FeO) at room

temperature.[53] In contrast, our results agree with reported variation in density of iron silicate glasses at room temperature[29,30] and also with that for iron oxide melts at temperatures above their liquidus.[54] Assuming the partial molar volumes of SiO_2 and Na_2O are fixed as reported values for NS66.0 composition (V_{SiO_2} = 26.0 cm^3/mol, V_{Na_2O} = 20.4 cm^3/mol),[55] the partial molar volumes of Fe_2O_3 ($V_{Fe_2O_3}$) and FeO (V_{FeO}) are determined to 38.8 and 10.7 cm^3/mol, respectively. The larger partial molar volume of Fe_2O_3 compared to that of FeO explains the increase in the molar volume due to iron oxidation. This is consistent with the general trend that framework cations increase the free volume of the glass structure (i.e., the molar volume).[56] Liu and Lange[57] estimated the partial molar volume of Fe_2O_3 in silicate melts at high temperatures: $V_{Fe_2O_3}$is approximately 45.5 cm^3/mol in case Fe^{3+} ions are four-fold coordinated, whereas $V_{Fe_2O_3}$ is close to 34 cm^3/mol when Fe^{3+} ions are six-fold coordinated. The obtained $V_{Fe_2O_3}$ (38.8 cm^3/mol) in the present NSF glasses is between the two end values. Also, obtained V_{FeO} value of 10.7 cm^3/mol is smaller than estimated V_{FeO} (14.6 cm^3/mol) in silicate melts at 1723 K when Fe^{2+} ions are in five-fold coordination.[58] The partial molar volumes of Fe_2O_3 and FeO in high-temperature melts have been correlated with the coordination numbers of iron ions; however, there are few reports[53] on their values in glass at room temperature. The influence of thermal expansion (i.e., vibrational and configurational contributions)[59] on $V_{Fe_2O_3}$ and V_{FeO} should be considered to precisely compare the obtained data with those reported for melts at high temperatures.

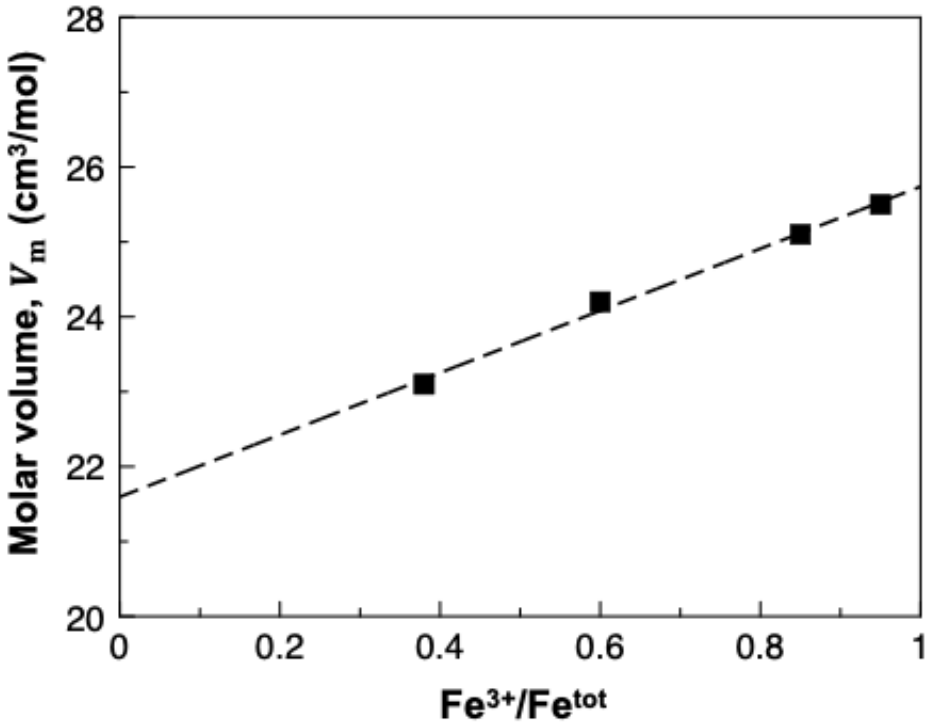

Figure 6 Effect of iron redox state (Fe^{3+}/Fe^{tot}) on the molar volume of the NSF glasses at room temperature. The dashed line represents the linear regression line.

4.3 T_g, fragility and configurational entropy

Temperature dependence of the viscosity has been empirically expressed using Tamman-Vogel-Flucher (TVF) model,[60] which is shown as Eq. (6):

$$\log \eta = A + \frac{B}{T - T_1}, \quad (6)$$

where A, B, and T_1 are the adjustable parameters. However, the physical meaning of these adjustable parameters is ambiguous. According to the theory of Adam and Gibbs[61] for

relaxation process, the viscosity can be linked to the configurational entropy ($S^{\mathrm{conf}}(T)$) which should change depending on the structural roles of iron ions. The following equation is used to calculate the configurational entropy[5,62]:

$$\log \eta = A_e + \frac{B_e}{T[S^{\mathrm{conf}}(T_{\mathrm{g}}) + \int_{T_{\mathrm{g}}}^{T} \frac{\mathrm{Cp}^{\mathrm{conf}}}{T dT}]}, \quad (7)$$

where A_e and B_e are adjustable parameters. $\mathrm{Cp}^{\mathrm{conf}}$ is the configurational heat capacity. **Table 3** lists the derived parameters of the TVF and Adams–Gibbs equations. The heat capacities of the liquids and glasses were calculated using the models proposed by Richet and Bottinga[63] and Richet[64] as reported by Neuville.[7] The $\mathrm{Cp}^{\mathrm{conf}}$ is calculated as the difference between the heat capacity of the glass at the glass transition temperature and the heat capacity of the liquid.[7] T_{g} is calculated for a viscosity equal to 12 log Pa·s, and the T_{g} of glass corresponds to a temperature region where the structure of the liquid is frozen on an experimental time scale,[65] then T_{g} can be an indicator of the rigidity of the glass structure. As shown in **Figure 7**, the T_{g} of the NSF glasses increased linearly with the Fe^{3+}/Fe^{tot} ratio. The attraction forth between iron and oxygen ions is proportional to $Z_{\mathrm{Fe}}Z_{\mathrm{O}}/L_{\mathrm{Fe-O}}^2$; the attraction for Fe^{3+}–O (1.66) is larger than that for Fe^{2+}–O (0.94), where Z_{Fe} and Z_{O} are the valence numbers of iron and oxygen ions, respectively. The calculated values indicate that Fe^{3+} cations are more strongly bonded to oxygen than are Fe^{2+} cations. The increase in T_{g} can be explained by an increase in the attraction between iron and oxygen ions owing to the oxidation of iron ions. This trend in T_{g} is consistent with the conclusion obtained by high-temperature Mössbauer spectroscopy that the relaxation time of the local structure in the neighborhood of Fe^{3+} is longer than that of Fe^{2+}. As shown in Figure 7,

Cp^{conf} increases slowly with the Fe^{3+}/Fe^{tot} ratio, whereas the configuration entropy, $S^{conf}(T_g)$, decreases with the Fe^{3+}/Fe^{tot}, This is in good agreement with the network-forming role of Fe^{3+}, which acts as a network former and decreases the disorder and configuration entropy of the glass while increasing T_g.

Table 3 TVF, AG parameters: data in K, J/mol, J/mol.K

	O2	Air	Ar	ArH_2
A	-11.66	-13.70	-11.35	-21.85
B*	8.17	9.24	7.22	17.81
T_1	374.4	342.7	379.1	127.2
T_g	719.7	702.3	688.4	654.0
*AAD***	0.04	0.01	0.02	0.03
Cp^{conf} ***	22.72	22.53	20.96	19.90
A_e	-1.73	-1.79	-2.02	-1.85
B_e*	79.50	7.29	80.01	77.29
$S^{conf}(T_g)$	8.05	8.20	8.35	8.52
AAD	0.03	0.03	0.04	0.03
T_0	504.	505.	500.	426.

*B and Be are divided by 1000

** average absolute deviation

*** values calculate using the Richet (1987) and Richet and Bottinga (1985) models and calculated Tg.

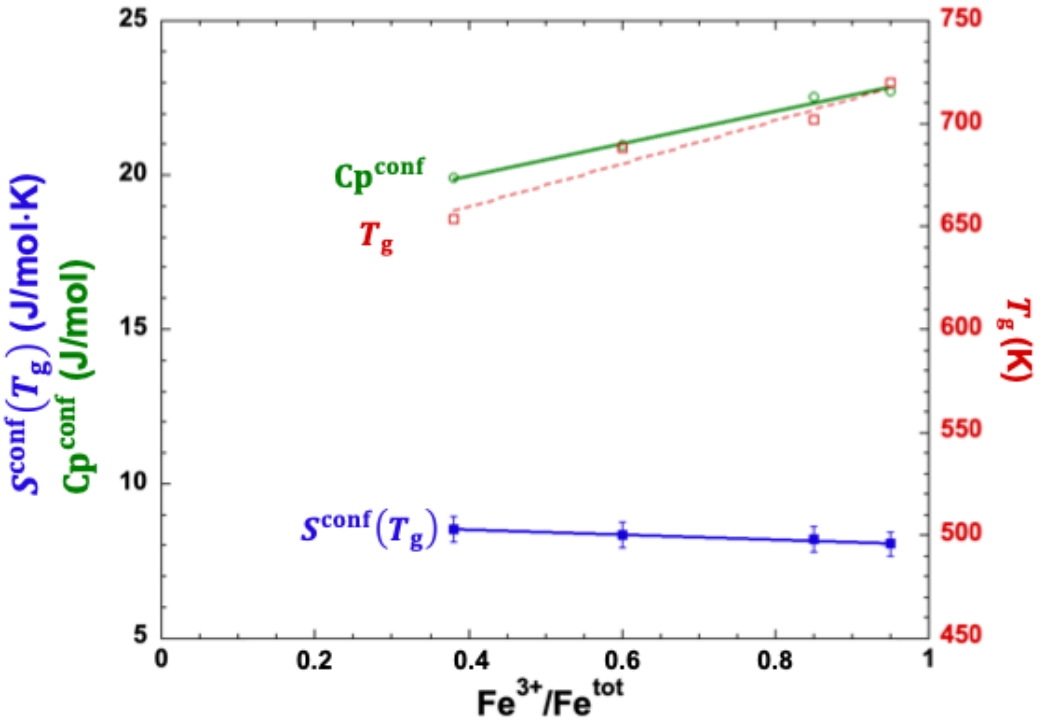

Figure 7 Cp^{conf}, $S^{conf}(T_g)$ and T_g as a function of the redox state of iron (Fe^{3+}/Fe^{tot}).

Because the liquid viscosity for many types of systems will reach approximately 10^{12} Pa·s when the temperature is close to T_g, the temperature dependence of the viscosity has been classified by viscosity variation against T_g scaled inverse temperature (T_g/T). Angell proposed a concept of "fragility," which will be an indicator of stability of microstructure against temperature;[66] viscosity changes linearly with T_g/T for the "strong" system whereas the "fragile" system is characterized by the large deviation from the linear relationship. Fragility (m) is defined as the slope of the log η against T_g/T at the glass transition temperature.[66] **Figure 8** a) shows the relationship between the viscosity (log η) for the NSF system and T_g/T compared with those for the NS66.0 and $32Na_2O$–$58SiO_2$-$10Al_2O_3$ (NA58.10) melts.[42] It was found that the fragility of NS66.0 decreases by adding alumina, whereas the sodium silicate melts became more fragile with the addition of iron oxides. This tendency implies that the aluminosilicate system has a stronger network structure than iron-silicate melts and glasses. It should also be noted that the fragility of the NSF system varied only slightly depending on the iron redox state in the range of Fe^{3+}/Fe^{tot} = 0.95 - 0.60. The fragility of NSF_Ar/H2 was lower than that of the other NSF glasses, and the fragility of the sample was close to that of NS66.0. It has been reported that the fragility of alkali silicate liquids slightly increases with an increase in network modifiers,[67] however, the fragility of alkali silicate liquids is more sensitive to the incorporation of another network former (e.g., B^{3+}) into the silicate network structure.[68] Figure 8 b) shows the evolution of fragility (m)

against the $B_2O_3/(SiO_2+B_2O_3)$ molar ratio, compared with that for the present NSF ($Na_2O\cdot 2SiO_2$–Fe_2O_3–FeO) system. As shown in the Figure 8 b), the fragility drastically increased with increasing $B_2O_3/(SiO_2+B_2O_3)$ molar ratio. Similarly, fragility of $Na_2O\cdot 2SiO_2$ melt increases by an increase of Fe_2O_3 (i.e., Fe^{3+}) concentration. This phenomenon indicates that Fe^{3+} cations behave as network formers like B^{3+} in this alkali-silicate system, whereas Fe^{2+} tends to be a network modifier in the present alkali-silicate melts.

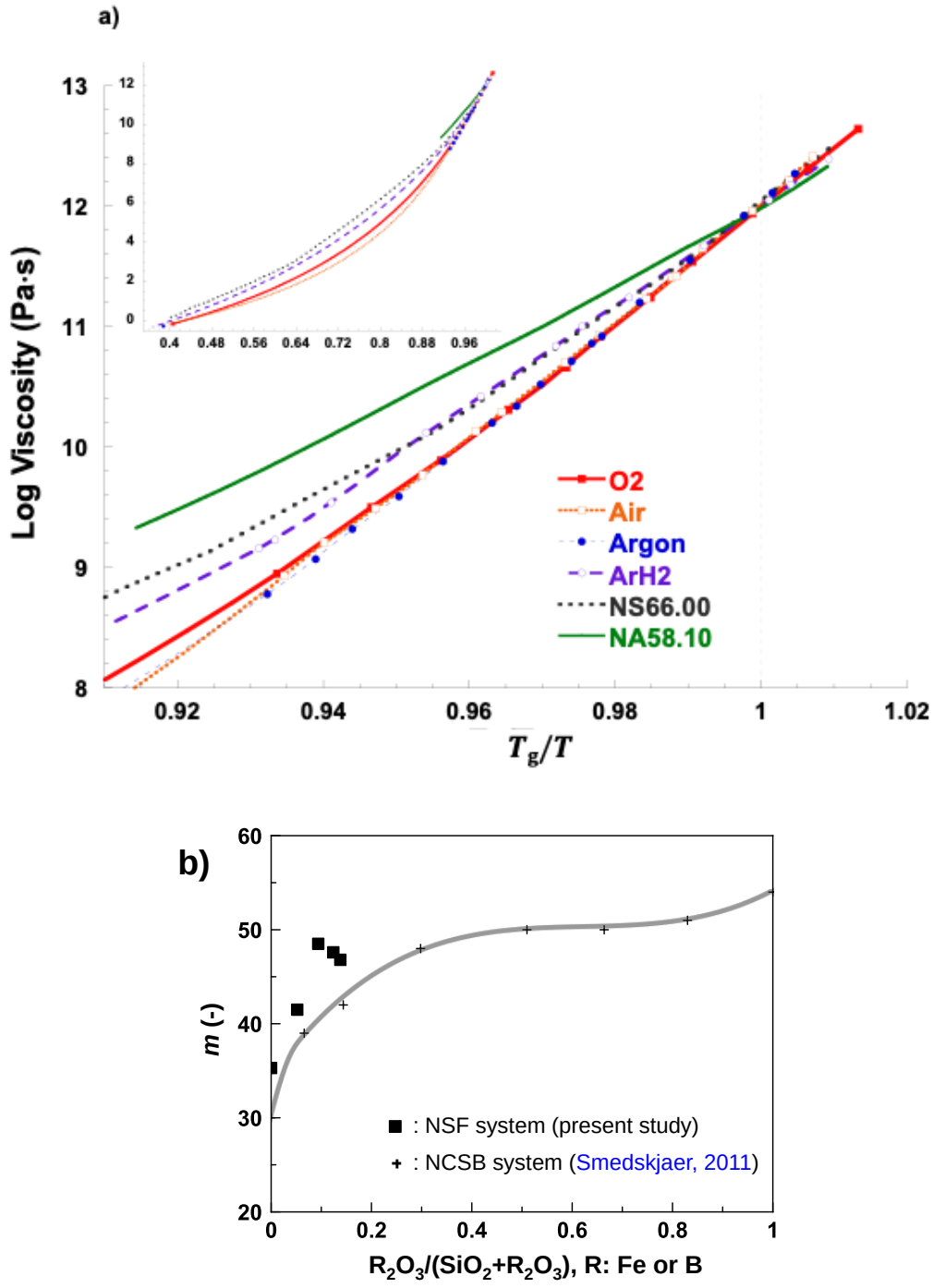

Figure 8 a) Relationship between viscosity and normalized temperature by T_g (T/T_g). b) Fragility (m) of NSF system with a variation of the molar ratio of $Fe_2O_3/(Fe_2O_3 + SiO_2)$ where Fe_2O_3 concentration is calculated from the Fe^{3+}/Fe^{tot} ratio determined by XANES experiments. The evolution of m value for the present NSF system is compared with that

for $15Na_2O–10CaO–(75\text{-}x)SiO_2\text{-}xB_2O_3$ (mol%) system, which was reported by Smedskjaer et al.[68]

Figure 9 clearly shows that viscosity increases as iron oxidizes, confirming Dingwell's published measurements at high temperature[20,21], which showed an increase of the order of 0.1 log units, but this new work shows that viscosity increases by more than 4 orders of magnitude close to T_g as Fe^{3+}/Fe^{tot} increases from 0.38 to 0.95. This increase is drastic and can be of enormous importance in industrial and volcanic processes, and results solely from the oxidation of iron at low temperatures without any nucleation or crystallization.

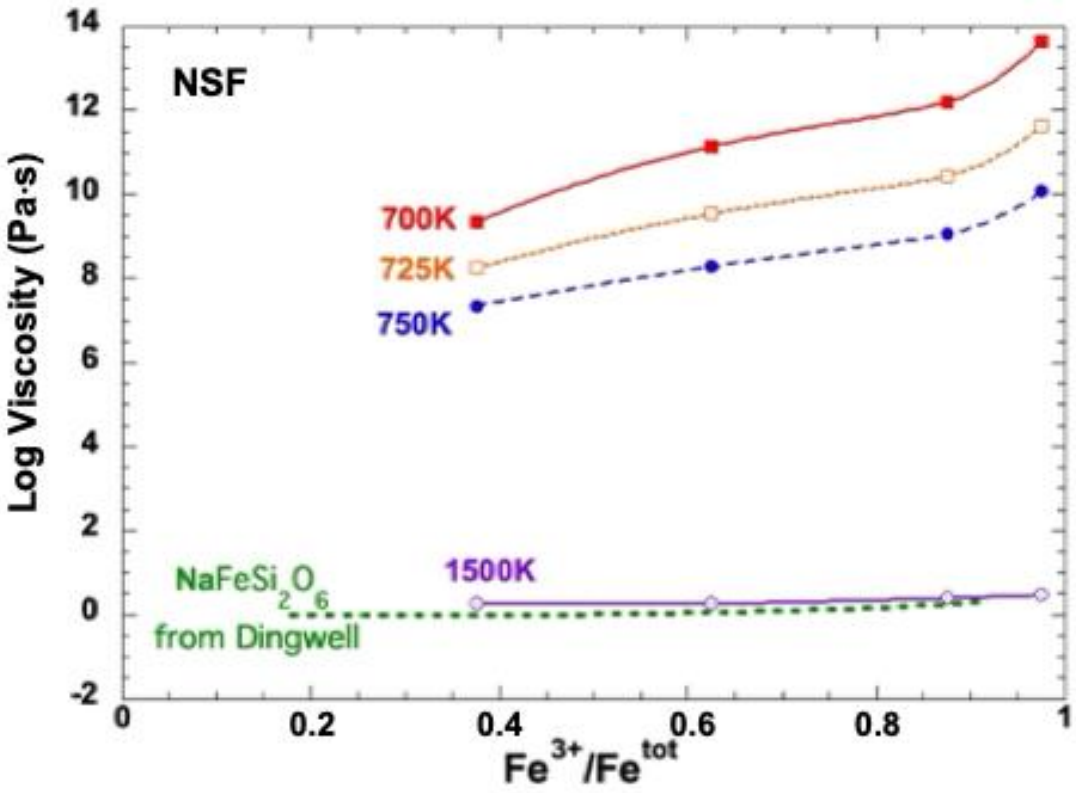

Figure 9 Isoviscosity as a function of Fe^{3+}/Fe^{tot} for the present NSF compositions, compared with reported data by Dingwell.[20,21]

5 Conclusion

This study evaluates the viscosity, density (molar volume), configurational entropy, iron redox state, and interatomic distance between iron and oxygen in a simple sodium iron silicate system with a variety of iron redox states. The following information was obtained from the present study:

A) The viscosity of the sodium iron silicate system was drastically increased by the oxidation of iron ions at temperatures close to their glass transition, whereas the viscosity changes at temperatures above their liquidus were small. Simultaneously, the configuration entropy at the glass transition temperature decreases. Fragility of $Na_2O{\cdot}2SiO_2$ melt increases with an increase of Fe_2O_3 concentration whereas influence of FeO on the fragility is small.

B) The partial molar volume of the NSF glasses at room temperature increases linearly with the Fe^{3+}/Fe^{tot} ratio. The estimated partial molar volume of Fe_2O_3 (38.8 cm^3/mol) is more than twice that of FeO (10.7 cm^3/mol).

C) Synchrotron X-ray total scattering demonstrated that the interatomic distance between iron and oxygen ($L_{\mathrm{Fe-O}}$) decreased with increasing Fe^{3+}/Fe^{tot} ratio of the NSF glasses. The variation in $L_{\mathrm{Fe-O}}$ results in an increase in the attraction between iron and oxygen ions, which explains the change in viscosity and T_{g} owing to the oxidation of iron ions.

Our findings indicated that Fe^{3+} ions act as a network former whereas Fe^{2+} ions tend to be as network modifiers. This conclusion is consistent with the results of previous studies. $L_{\mathrm{Fe-O}}$ and density of the NSF system with variations in the iron redox state at elevated

temperatures should be examined in future studies to determine the coordination structure of iron ions in their super-cooled liquids and melts.

Acknowledgment

This study was partially supported by JSPS KAKENHI JP16H04543 and JP25420792. S.S. would like to thank “Institut de Physique du Globe de Paris (IPGP)” and “Université Paris Diderot “ for their financial supports (for S.S.) to make progress on this work as an international collaboration. We acknowledge SOLEIL for provision of synchrotron radiation facilities and we would like to thank Dr Nicolas Trcera for assistance in using beamline “LUCIA” for the x-ray absorption spectroscopy. Synchrotron X-ray total scattering experiments were performed at BL04B2 of Spring-8 with the approval of the Japan Synchrotron Radiation Research Institute (JASRI) (Proposal No. 2017B1400). This work was performed under the Research Programs of “Five-star Alliance” in HJRC Mater. & Dev.

Author contributions

S. S., H. S., and D. R. N. designed and initiated this study. S.S. and H.S. prepared glass samples with various iron redox states at Tohoku University, Japan. D.R.N. conducted viscosity measurements at temperatures close to the glass transition temperature at the IPGP, France. M.R.C. and D.R.N. observed the redox states of the samples using Fe-kedge XAS in the Synchrotron Soleil (LUCIA), France. S. S. and D. R. N. collected the Raman spectra and densities of the samples from IPGP, France. H.Y., T.W., S.S., and K.O. performed synchrotron

X-ray total scattering experiments at Spring-8 (BL04B2), Japan. All the authors commented on the manuscript.

References

1. Dingwell DB. Transport properties of magmas: Dissusion and rheology. Elements. 2006:2(5);281–286. 10.2113/gselements.2.5.281.
2. Mills KC. Metallurgical slags. Encyclopedia of glass science, technology, history, and culture (eds Richet P, Conradt R, Takada A, Dyon J.). Wiley-American Ceramic Society. Hoboken, NJ. 2021. 10.1002/9781118801017.ch7.4.
3. Krüger S, Deubener J. Lag time to crystal nucleation of supercooled lithium disilicate melts: A test of the classical nucleation theory. J Non-Cryst Solids. 2015:426;1–6. 10.1016/j.jnoncrysol.2015.06.023.
4. Bockris JO, Mackenzie JD, Kitchener JA. Viscous flow in silica and binary liquid silicates. Trans Faraday Soc. 1955;51:1734–1748. 10.1039/tf9555101734.
5. Neuville DR, Richet P. Viscosity and mixing in molten (Ca, Mg) pyroxenes and garnets. Geochim Cosmochim Acta 1991;55(4):1011–1019. 10.1016/0016-7037(91)90159-3.
6. Neuville DR. Structure and properties in (Sr, Na) silicate glasses and melts. Phys Chem Glasses. 2005:46;112–118.
7. Neuville DR. Viscosity, structure and mixing in (Ca, Na) silicate melts. Chem Geol. 2006: 229(1–3);28–41. 10.1016/j.chemgeo.2006.01.008.
8. Novikov AN, Neuville DR, Hennet L, Gueguen Y, Thiaudiere D, Charpentier T, Florian P. Al and Sr environment in tectosilicate glasses and melts: Viscosity, Raman and NMR investigation. Chem Geol. 2017:461;115–127. 10.1016/j.chemgeo.2016.11.023.
9. Toplis MJ, Dingwell DB, Hess KU, Lenci T. Viscosity, fragility, and configurational entropy of melts along the join SiO_2-$NaAlSiO_4$. Am Mineral. 1997:82;979–990.
10. Genova D, Kolzenburg S, Wiesmaier S, Dallanave E, Neuville DR, Hess KU, Dingwell DB. A compositional tipping point governing the mobilization and eruption style of rhyolitic magma. Nature. 2017:552;235–238. 10.1038/nature24488.
11. Hess KU, Dingwell DB, Gennaro C, Mincione V. Viscosity-temperature behaviour of dry melts in the Qz-Ab-Or system. Chem Geol. 2001:174(1–3);133–142. 10.1016/S0009-2541(00)00312-0.
12. Neuville DR, Courtial P, Dingwell DB, Richet P. Thermodynamic and rheological properties of rhyolite and andesite melts. Contrib Mineral Petrol. 1993:113;572–581. 10.1007/Bf00698324.
13. Sukenaga S, Gueguen Y, Celarie F, Rouxel T, Tashiro M, Yoshida S, Saito N, Nakashima K, Shibata H. Effect of calcium and potassium oxide addition on the viscosity and fragility of a calcium aluminosilicate melt. J Am Ceram Soc. 2024:107(6);3822–3836. 10.1111/jace.19722.

14. Giordano D, Russell JK, Dingwell DB. Viscosity of magmatic liquids: A model. Earth Planet Sci Lett. 2008:271(1–4);123–134. 10.1016/j.epsl.2008.03.038.
15. LeLosq C, Neuville DR. Molecular structure, configurational entropy and viscosity of silicate melts: Link through the adam and gibbs theory of viscous flow. J Non-Cryst Solids 2017 :463;175–188. 10.1016/j.jnoncrysol.2017.02.010.
16. Giordano D, Russell JK. Towards a structural model for the viscosity of geological melts. Earth Planet Sci Lett. 2018:501;202–212. 10.1016/j.epsl.2018.08.031.
17. Moretti R, Ottonelo G. Silicate melt thermochemistry and the redox state of magmas. Geochimical melts. Rev Mineral Geochem. 2022:87(1);339–403. 10.2138/rmg.2022.87.08.
18. Hayashi M, Horita K, Endo R, Watanabe T, Susa M. Effect of coordination structure of iron ions on iron oxide activities in Na_2O–SiO_2–FeO–Fe_2O_3 melts. ISIJ Int. 2019:59(10);1744–1751. 10.2355/isijinternational.ISIJINT-2019-097.
19. Kress VC, Carmichael ISE. The compressibility of silicate liquids containing Fe_2O_3 and the effect of composition, temperature, oxygen fugacity and pressure on their redox states. Contrib Mineral Petrol. 1991:108;82–92. 10.1007/Bf00307328.
20. Dingwell DB. Redox viscometry of some Fe-bearing silicate melts. Am Mineral. 1991:76; 1560–1562.
21. Dingwell DB, Virgo D. The effect of oxidation-state on the viscosity of melts in the system Na_2O–FeO–Fe_2O_3-SiO_2. Geochim Cosmochim Acta 1987:51(2);195–205. 10.1016/0016-7037(87)90231-6.
22. Cicconi MR, De Ligny D, Gallo TM, Neuville DR. Ca neighbors from xanes spectroscopy: A tool to investigate structure, redox, and nucleation processes in silicate glasses, melts, and crystals. Am Mineral. 2016:101;1232–1235. 10.2138/am-2016-5663.
23. Weigel C, McCammon C, Keppler H. High-temperature Mössbauer spectroscopy: A probe for the relaxation time of fe species in silicate melts and glasses. Am Mineral. 2010:95(11–12); 1701–1707. 10.2138/am.2010.3490.
24. Bouhifd MA, Richet P, Besson P, Roskosz M, Ingrin J. Redox state, microstructure and viscosity of a partially crystallized basalt melt. Earth Planet Sci Lett. 2004:218(1–2);31–44. 10.1016/S0012-821x(03)00641-1.
25. Cukierman M, Uhlmann DR. Effects of iron oxidation-state on viscosity, lunar composition 15555. J Geophys Res. 1974:79(11);1594–1598. 10.1029/JB079i011p01594.
26. Liebske C, Behrens H, Holtz F, Lange RA. The influence of pressure and composition on the viscosity of andesitic melts. Geochim Cosmochim Acta. 2003:67(3);473–485. 10.1016/S0016-7037(02)01139-0.
27. Stabile P, Webb S, Knipping JL, Behrens H, Paris E, Giuli G. Viscosity of pantelleritic and alkali-silicate melts: Effect of Fe redox state and Na/(Na + K) ratio. Chem Geol. 2016:442; 73–82. 10.1016/j.chemgeo.2016.09.003.
28. Klein LC, Fasano BV, Wu JM. Flow behavior of ten iron-containing silicate compositions. Proceedings of the 12th Lunar and Planetary Science Conference. 1981:12B;1759–1767.

29. Klein LC, Fasano BV, Wu JM. Viscous flow behavior of four iron-containing silicates with alumina, effects of composition and oxidation condition. J Geophys Res. 1983:88(S02);A880–A886. 10.1029/JB088iS02p0A880.
30. Montenero A, Friggeri M, Giori DC, Belkhiria N, Pye LD. Iron soda silica glasses - preparation, properties, structure. J Non-Cryst Solids. 1986:84(1–3);45–60. 10.1016/0022-3093(86)90761-1.
31. Osugi T, Sukenaga S, Inatomi Y, Gonda Y, Saito N, Nakashima K. Effect of oxidation state of iron ions on the viscosity of alkali silicate melts. ISIJ Int. 2013:53(2);185–190. 10.2355/isijinternational.53.185.
32. Cicconi MR, Giuli G, Ertel-Ingrisch W, Paris E, Dingwell DB. The effect of the [Na/(Na + K)] ratio on Fe speciation in phonolitic glasses. Am Mineral. 2015:100(7);1610–1619. 10.2138/am-2015-5155.
33. Kohara S, Itou M, Suzuya K, Inamura Y, Sakurai Y, Ohishi Y, Takata M. Structural studies of disordered materials using high-energy X-ray diffraction from ambient to extreme conditions. J Phys Condens Matter. 2007:19;506101(1-15). 10.1088/0953-8984/19/50/506101.
34. Kohara S, Salmon PS. Recent advances in identifying the structure of liquid and glassy oxide and chalcogenide materials under extreme conditions: A joint approach using diffraction and atomistic simulation. Adv Phys X. 2016:1;640–660. 10.1080/23746149.2016.1232177.
35. Neuville DR, De Ligny D, Henderson GS. Advances in Raman spectroscopy applied to earth and material sciences. Rev Mineral Geochem. 2014:78;509–541. 10.2138/rmg.2013.78.13.
36. Shimodaira N, Saito K, Hiramitsu N, Matsushita S, Ikushima AJ. Effects of fictive temperature and halogen doping on the boson peak in silica glass. Phys Rev B. 2005:71; 024209. https://doi.org/10.1103/PhysRevB.71.024209.
37. Cicconi MR, Neuville DR, Blanc W, Lupi JF, Vermillac M, De Ligny D. Cerium/aluminum correlation in aluminosilicate glasses and optical silica fiber preforms. J Non-Cryst Solids. 2017:475;85–95. 10.1016/j.jnoncrysol.2017.08.035.
38. El Hayek R., Pisch A., Ferey F., Cicconi M.R., Vantelon D., and Neuville D.R. (2024) Role of iron on calcium aluminate glasses and melts. Glass Europe. In press
39. Mysen BO, Seifert F, Virgo D. Structure and redox equilibria of iron-bearing silicate melts. Am Mineral. 1980:65;867–884.
40. Sasaki Y, Mohri M, Suyama K, Ishii K. The effect of Fe^{3+} ions on the anionic structure of iron-bearing sodium silicate melts. ISIJ Int. 2000:40(12);1181–1187. 10.2355/isijinternational.40.1181.
41. Magnien V, Neuville DR, Cormier L, Roux J, Pinet O, Richet P. Kinetics of iron redox reactions: A high-temperature XANES and Raman spectroscopy study. J Nucl Mater. 2006:352(1–3);190–195. 10.1016/j.jnucmat.2006.02.053.
42. Cochain B, Neuville DR, Henderson GS, McCammon C, Pinet O, Richet P. Iron content, redox state and structure of sodium borosilicate glasses: A Raman, Mössbauer and

boron K-edge XANES spectroscopy study. J Am Ceram Soc. 2012:94(3);1–12. 10.1111/j.1551-2916.2011.05020.x.

43. Welsch AM, Knipping JL, Behrens H. Fe-oxidation state in alkali-trisilicate glasses - a Raman spectroscopic study. J Non-Cryst Solids. 2017:471;28–38. 10.1016/j.jnoncrysol.2017.04.033.
44. Neuville DR, Cicconi MR, Le Losq C. How measure the oxidation state of multiovalent elements in mrals, glasses, and melts?. Magma Redox Geochemistry. AGU Geophysical Monography Series (eds Moretti R and Neuville DR). American Geophysical Union. John Wiley & Sons, Inc. Hoboken, HJ. 2021. 10.1002/9781119473206.ch13.
45. El Hayek R, Pisch A, Ferey F, Cicconi MR, Vantelon D, Neuville DR. Role of iron on calcium aluminate glasses and melts. Glass Europe. 2024. In press.
46. Brown GE, Farges F, Calas G. X-ray scattering and x-ray spectroscopy studies of silicate melts. Structure, Dynamics, and Properties of Silicate Melts (eds Stebbins JF, McMillan PF, Dingwell DB). Rev Mineral. Mineralogical Society of America, Washington, D.C. 1995:32;317–410. 10.1515/9781501509384-011.
47. Neuville DR, Cormier L, Massiot D. Al coordination and speciation in clacium aluminosilicate glasses: Effects of composition determined by ^{27}Al MQ-MAS NMR and Raman spectroscopy. Chem Geol. 2006:229;173–185. 10.1016/j.chemgeo.2006.01.019.
48. Kim H-I, Lee SK. Extent of disorder in iron-bearing albite and anorthite melts: Insights from multi-nuclear (^{29}Si, ^{27}Al, and ^{17}O) solid-state NMR study of iron-bearing $NaAlSi_3O_8$ and $CaAl_2Si_2O_8$ glasses. Chem Geol. 2020:538;119498. 10.1016/j.chemgeo.2020.119498.
49. Holland D, Mekki A, Gee IA, McConville CF, Johnson JA, Johnson CE, Appleyard P, Thomas M. The structure of sodium iron silicate glass - a multi-technique approach. J Non-Cryst Solids. 1999:253;192–202. 10.1016/S0022-3093(99)00353-1.
50. Jackson WE, Farges F, Yeager M, Mabrouk PA, Rossano S, Waychunas GA, Solomon EI, Brown GE. Multi-spectroscopic study of Fe(II) in silicate glasses: Implications for the coordination environment of Fe(II) in silicate melts. Geochim Cosmochim Acta. 2005:69; 4315–4332. 10.1016/j.gca.2005.01.008.
51. Weigel C, Cormier L, Galoisy L, Calas G, Bowron D, Beuneu B. Determination of Fe^{3+} sites in a $NaFeSi_2O_6$ glass by neutron diffraction with isotopic substitution coupled with numerical simulation. Appl Phys Lett. 2006:89;141911. 10.1063/1.2359532.
52. Henderson GS. The structure of silicate melts: A glass perspective. Can Mineral. 2005:43; 1921–1958. 10.2113/gscanmin.43.6.1921.
53. Knipping JL, Behrens H, Wilke M, Gottlicher J, Stabile P. Effect of oxygen fugacity on the coordination and oxidation state of iron in alkali bearing silicate melts. Chem Geol. 2015: 411;143–154. 10.1016/j.chemgeo.2015.07.004
54. Mori K, Suzuki K. Density of iron oxide melt in equilibrium with CO_2-CO gas mixture. Tetsu-to-Hagané. 1968:54;1123–1127.
55. Callow RJ. Partial molar volumes in alkali oxide-silica systems. J Soc Glass Technol. 1952: 36;137–141.

56. Kohara S, Ohno H, Takata M, Usuki T, Morita H, Suzuya K, Akola J, Pusztai L. Lead silicate glasses: Binary network-former glasses with large amounts of free volume. Phys Rev B. 2010:82;134209 (1–7). 10.1103/PhysRevB.82.134209.
57. Liu Q, Lange RA. The partial molar volume of Fe_2O_3 in alkali silicate melts: Evidence for an average Fe^{3+} coordination number near five. Am Mineral. 2006:91;385–393. 10.2138/am.2006.1902.
58. Guo X, Lange RA, Ai YH. Density and sound speed measurements on model basalt (An-Di-Dd) liquids at one bar: New constraints on the partial molar volume and compressibility of the Feo component. Earth Planet Sci Lett. 2014:388;283–292. 10.1016/j.epsl.2013.12.005.
59. Potuzak M, Mauro JC, Kiczenski TJ, Ellison AJ, Allan DC. Communication: Resolving the vibrational and configurational contributions to thermal expansion in isobaric glass-forming systems. J Chem Phys. 2010:133;091102. https://doi.org/10.1063/1.3481441
60. Fulcher GS. Analysis of recent measurements of the viscosity of glasses. J Am Ceram Soc. 1925:8(6);339–355. 10.1111/j.1151-2916.1925.tb16731.x.
61. Adam G, Gibbs JH. On the temperature dependence of cooperative relaxation properties in glass-forming liquids. J Chem Phys. 1965.43(1);139–146. 10.1063/1.1696442.
62. Richet P. Viscosity and configurational entropy of silicate melts. Geochim Cosmochim Acta. 1984:48;471–483. 10.1016/0016-7037(84)90275-8.
63. Richet P, Botting Y. Heat capacity of aluminum-free liquid silicates. Geochim Cosmochim Acta. 1985:49(2);471–486. 10.1016/0016-7037(85)90039-0.
64. Richet P. Heat capacity of silicate glasses. Chem Geol. 1987:62(1–2);111–124. 10.1016/0009-2541(87)90062-3.
65. Cormier L, Neuville DR, Calas G. Relationship between structure and glass transition temperature in low-silica calcium aluminosilicate glasses: The origin of the anomaly at low silica content. J Am Ceram Soc. 2005:88(8);2292–2299. 10.1111/j.1551-2916.2005.00428.x.
66. Angel CA. Structural instability and relaxation in liquid and glassy phases near the fragile liquid limit. J Non-Cryst Solids. 1988:102;205–221. 10.1016/0022-3093(88)90133-0.
67. Sidebottom DL. The fragility of alkali silicate glass melts : part of a universal topological pattern. J Non-Cryst Solids. 2019:516;63–66. 10.1016/j.noncrysol.2019.04.033
68. Smedskjaer MM, Mauro JC, Youngman RE, Hogue CL, Potuzak M, Yue Y. Topological principles of borosilicate glass chemistry. J Phys Chem B. 2011:115;12930–12946. 10.1021/jp208796b

Caption list

Table 1 Analyzed compositions (as mol%, recalculated from wet chemical analysis) and properties of the glasses. Nominal composition should be $54.6SiO_2$–$27.2Na_2O$–18.2FeO (mol%) when iron oxide concentration is calculated as FeO.

Table 2 a) Viscosity measurements at low temperature, temperature in Kelvin, and viscosity in log Pa·s. b) Viscosities at high temperature (1773 K) reported by Osugi et al.[31]

Table 3 TVF, AG parameters: data in K, J/mol, J/mol.K

Figure 1 a) XANES at the Fe K-edge of the NSF glasses, obtained at room temperature. b) Fitting results of the pre-edge peak of the XANES spectra. Numbers on the figure displays the ratio of Fe^{3+} to total-iron (Fe^{3+}/Fe^{tot}).

Figure 2 Viscosities of the sodium-iron-silicate melts as a function of reciprocal temperature. Literature data[7] of NS66.0 is plotted for comparison. Inset: logarithmic viscosity vs reciprocal temperature near glass transition.

Figure 3 Raman spectra of the Na_2O–SiO_2–Fe_xO (NSF) glasses, which were prepared in a variety of atmospheres, compared with that of NS66.0 glass.

Figure 4 Total correlation function ($T(r)$) of the NSF glasses, compared with that of NS66.0 glass at room temperature.

Figure 5 Influence of iron redox state (Fe^{3+}/Fe^{tot}) on the interatomic distance between iron and oxygen ($L_{\mathrm{Fe-O}}$) in the NSF glasses at room temperature. The $L_{\mathrm{Fe-O}}$ was determined by a Gaussian fit to the $T(r)$. The numbers in the figure shows the estimated $L_{\mathrm{Fe\text{-}O}}$ at the two end points when Fe^{3+}/Fe^{tot} = 0 and 1.

Figure 6 Effect of iron redox state (Fe^{3+}/Fe^{tot}) on the molar volume of the NSF glasses at room temperature. The dashed line represents the linear regression line.

Figure 7 Cp^{conf}, $S^{conf}(T_g)$ and T_g as a function of the redox state of iron (Fe^{3+}/Fe^{tot}).

Figure 8 a) Relationship between viscosity and normalized temperature by T_g (T/T_g). b) Fragility (m) of NSF system with a variation of the molar ratio of $Fe_2O_3/(Fe_2O_3 + SiO_2)$ where Fe_2O_3 concentration is calculated from the Fe^{3+}/Fe^{tot} ratio determined by XANES experiments. The evolution of m for NSF system is compared with that for $15Na_2O–10CaO–(75\text{-}x)SiO_2\text{-}xB_2O_3$ system, which was reported by Smedskjaer et al.[68]

Figure 9 Isoviscosity as a function of Fe^{3+}/Fe^{tot} for the present NSF compositions, compared with reported data by Dingwell.[20,21]